Thermal response of building stones contaminated with salts

Céline Thomachot-Schneider, Patricia Vázquez, Maxime Gommeaux, Norman Lelarge, Alexandra Conreux, Xavier Drothière, Kamel Mouhoubi, Jean-Luc Bodnar

Thermal response of building stones contaminated with salts.

Céline Thomachot-Schneider[1]*, Patricia Vázquez[1], Maxime Gommeaux[1], Norman Lelarge[1], Alexandra Conreux[1], Xavier Drothière[1], Kamel Mouhoubi[2], Jean-Luc Bodnar[2]

[1]GEGENAA, EA 3795, Université de Reims Champagne-Ardenne, Reims, France

[2]CATHERM, GRESPI EA 4694, Université de Reims Champagne-Ardenne, Reims (France)

*: Corresponding author

Céline Thomachot-Schneider, GEGENAA, 2 esplanade Roland Garros, 51100 Reims, France

celine.schneider@univ-reims.fr

Graphical abstract:

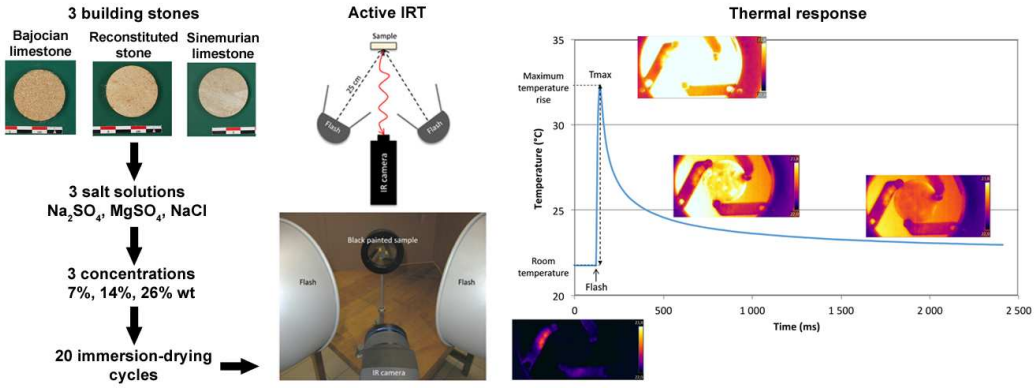

Highlights:

- Salt-contaminated stones were characterized by active infrared thermography (IRT).
- Salt uptake mass and location depended on stone type and on salt type and concentration.
- Active IRT helps determining salt type and concentration non-destructively and at early stages.

Keywords: salt weathering, building stone, active infrared thermography, NaCl, Na_2SO_4, $MgSO_4$

Abstract (150-250 words)

The accumulation of salts in building stones can lead to weathering features such as scaling, sanding or even slab detachment. To detect salts in walls at the early stages and to predict their evolution, the non-destructive technique (NDT) Infrared Thermography (IRT) was tested in a stimulated way. The main objective was to trial this technique in order to obtain more information such as the type of salt, its precise location and its concentration in building stones.

Three building materials were studied, including two natural limestones and a reconstituted stone. Samples were submitted to immersion/drying tests in water and in salt solutions of Na_2SO_4, NaCl and $MgSO_4$ at 7%, 14% and 26% in weight during 20 cycles of 24h. The weight of the samples and the surface colour were recorded after each cycle. After 1, 5, 10 and 15 cycles, 3 samples were taken out for active IRT measurements.

The results showed that when the porosity and the capillarity are low, the intake of salts into the porous network is low and the thermal response of the stone to heating (ΔT_{max}) corresponds to the salt thermal signature and has no relation with concentration. On the other hand, when the initial porosity is high, salts crystallize inside the porous network and porosity decreases. Hence, the thermal response of the porous stone is related to salt concentration and the ΔT_{max} increases until the stone starts to disaggregate.

Active IRT is a promising NDT adapted to identify and quantify salts within building stones during the first states of accumulation.

Introduction

Salt crystallization is a weathering process encountered in building stones in several environments such as coastal or urban areas. It occurs in different architectural positions such as the basement where capillary solutions rise from the ground [1] or sheltered parts as cornices where air pollution and sea salts can accumulate and react with the stone without being washed [2-4]). Weathering features caused by the presence of salts are numerous: figures of discolouration and deposit as moist area, black crust, efflorescences or subflorescences; figures due to material loss as powdering, alveolization or erosion; figures of detachment such as disintegration or scaling [5-7]. Except for efflorescences, which are superficial, salt weathering features only become visible when a large amount of salt has accumulated within the stone (either by leaching into the stone through wetting drying cycles or by capillary rise…), such that decontamination is difficult, and damage is irreversible. Therefore, it becomes necessary to detect these salts before an irreversible decay occurs.

Several types of salts can be found in building stones [8,9]: especially sulfates but also chlorides and nitrates. Sources of salts are diverse: they can originate from the material itself through its condition of formation (evaporites) or crafting (insufficiently crushed clinker, gypsum added to cement in too high concentration, wrong mixing or inappropriate aggregate choice). They can come from external sources through capillary rise of solutions rich in salts (natural salts or anthropic discharges such as sea spray or deicing salts for chlorides [10], pesticides, fertilizers for nitrates and sulfates) or through air pollution due to waste from the combustion of fossil fuels [2,11].

Sulfates, especially sodium sulfate (Na_2SO_4) and magnesium sulfate ($MgSO_4$) are known as the most aggressive salts [12], even though there are exceptions depending on the type of stones and experiments [13]. These salts have both several hydrated forms with different solubilities. They lead to different weathering patterns according to their differences in their

properties and crystallization behaviour: Na_2SO_4 generally produces scaling by crystallizing in the largest pores of the stone near the surface while $MgSO_4$ mainly causes the development of cracks by filling all the pores [14].

Sodium chloride is usually the least destructive salt in the numerous experimental studies performed with this salt [15,16]. It is a very soluble salt that tends to crystallize on the stone surface forming efflorescences and that produces damages mainly on the first millimetres [17].

Salt weathering features depend not only on the salt origin and the architectural position, but also on the behaviour of stone to wetting-drying. A building material with a porous network allowing it to have high capillary transfer with a high saturation but a slow drying that mainly occurs in depth, will be prone to slab detachment due to salt crystallization [18-21]. The pore size distribution (PSD) is considered to be the main factor that controls the salt uptake and the salt solution transfer in the material [20,22]. A building material that has low capillary transfer and that dries fast, usually used for the basement of monuments, is typically not sensitive to salt crystallization. However, a stone with low porosity but essentially microporosity can be prone to salt crystallization [23-26]. The upper limit of size of micropores facilitating the salt damage varies with authors from 0.05 to 5 μm [20,25,27-32].

On a monument, several types of stones with various petrophysic properties can be found. Their size, shape, architectural position and their exposition can vary a lot since it is usually huge in size and height and has a long history of construction, sometimes deconstruction and reconstruction and restoration phases. Due to the differences in stone types with different porosities and in weathering degrees due to different ages of positioning, a detailed study of salt distribution is needed in order to prevent and to organize the restoration phases. Given that salts generally accumulate at various depths below the stone surface, methods based on micro-drilling have been developed in order to minimize artificial damage [33,34]. This

technique gives only point data and numerous samplings are required. Furthermore, it is not a direct measurement since the concentration of salts has to be analysed afterwards in the laboratory and this method still can be considered as destructive. It is necessary to use non-destructive techniques (NDT) on building, especially on prestigious monument. Among these NDT, infrared thermography (IRT) is currently under development for this purpose [35-38]. This technique provides real-time surface measurements without contact and consequently destruction, and allows detecting defects or problem areas that may be invisible to the naked eye [39-44]. Its ability for inspection is only limited to a certain depth of the target to subsurface defect detection [45,46]. It is usually used in passive mode by recording the thermal radiation emitted by the surface of the body under natural conditions to detect defects, microcracks, moisture or salt presence [47-50]. This method is a rapid technique but mainly qualitative [45]. In the case of salt detection, the thermal anomaly is mainly due to the moisture that salts maintain in the walls [46,50-54] and passive IRT is thus limited to the detection of large amount of hygroscopic salts or to the study of crystallization processes [55,56]. To enhance the contrast and ease comparison, it is convenient to use IRT in an active mode by exciting the material with a source of heat (lamps, oven or hot packs) to induce measurable thermal response of the material [45,51,52,57-60]. Two types of active thermography exist: pulsed thermography (PT) and lock-in thermography (LT). PT is performed by thermal simulation of the surface of the material by a heating pulse, as used in the present study by flash illumination. The temperature variation of the surface is recorded during both heating and cooling phases. The heat propagation depends on material properties such as density, heat capacity and thermal conductivity [61]. Inhomogeneities like cracks or voids have different thermal properties from the material and can thus be detected. This technique is the most popular one in building diagnostics because of its rapidity and efficiency [45]. The LT uses longer heating that can be performed with a heating lamp

(Optical Lock-in Thermography OLT) or with elastic waves (Ultrasound Lock-in Thermography ULT). The LT technique is more effective in detecting thin defects deeper in comparison to PT.

The question is to know if this technique is able to provide, in addition to the presence of salts, information about the type of salt and its concentration. To this purpose, the study was conducted by testing 3 types of building materials of the North-East of France and the South of Wallonia (Belgium): two natural limestones and a reconstituted stone made with debris of the natural ones. These materials have been submitted to wetting-drying cycles in 3 salt solutions (Na_2SO_4, $MgSO_4$ et NaCl) at 3 different concentrations (7%, 14% and 26% in weight) and then assessed by active IRT.

2. Materials and methods

2.1. Materials

Three building stones were studied: two natural limestones from the Jurassic layers of the boundary of the Paris basin that straddle the border between France and Belgium, and a reconstituted stone (RS) made with debris of these limestones and a binding phase that is not known in detail from historic sources. The natural limestones are a Bajocian limestone (BJ, Lower Jurassic, ca. 180 Ma, LGW Figure 1) and a Sinemurian limestone (SN, (Lower Jurassic, ca. 200 Ma, LUX Figure 1).

Figure 1: Geological map of South of Wallonia (Belgium) showing location of the Orval abbey partially built with reconstituted stone (RS) and natural limestones from the Sinemurian (SN - LUX) and Bajocian (BJ - LGW) formations surrounding.

The two natural stones are used simultaneously in buildings of South of Wallonia (Belgium) as their color and origin are close to each other (Figure 2).

The reconstituted stone is known only from the Orval Abbey, where it was produced and used as an imitation of the natural stones for the building of parts of the modern Abbey (Figure 1,2).

The petrophysical properties of the three stone types have been measured in a previous study [19].

Figure 2: Example of monument mainly built with reconstituted stone and natural stones: a) Medieval ruins of the Orval Abbey built with Bajocian (BJ) and Sinemurian (SN) limestones; b) Modern part of the Orval Abbey built in last 1936 with the natural stones BJ and SN and reconstituted stones (RS); c) and d) Macroscopical view of the three building stones in the modern part.

The Bajocian limestone (BJ) is a bioclastic limestone rich in echinoderms with a high total porosity (31.1%) mainly made of macropores (Table 1). Its capillary kinetics is high (96.6 $g.m^{-2}.s^{-1/2}$) with a capillary saturation of 63%. The Sinemurian limestone (SN) is a siliceous limestone with the lowest porosity (7.6%) and transfer properties (7.3 $g.m^{-2}.s^{-1/2}$): its capillary saturation is 55% while its drying flow is -1315 $g.m^{-2}.s^{-1}$. The reconstituted stone (RS) is made of debris of the two natural stones. The RS is microporous, its porosity and capillary kinetics are intermediary to the two other stones (28.2% of porosity and weight increase coefficient of 66.3 $g.m^{-2}.s^{-½}$) while its capillary saturation (92.9%) and drying kinetics (-2250 $g.m^{-2}.s^{-1}$) are the highest.

On site, it presents mainly weathering patterns due to salts such as of moist areas, efflorescences, powdering and flaking of the surface in the capillary zones and due to frost action such as cracking of blocks [19,62,63]. The two natural limestones (BJ and SN) are less prone to salt weathering and biological colonisation is the main weathering pattern observed.

Table 1: Silicium/Calcium ratio (ICP-ES) and stone properties: water and mercury porosimetry (Pm<0.1 and Pm<5 correspond to the percentage of porosity filled up at the pressure corresponding to the pore access of respectively 0.1 µm and 5 µm); capillary absorption and drying kinetics.

		Bajocian limestone (BJ)	Reconstituted stone (RS)	Sinemurian limestone (SN)
Si/Ca		0.02	0.14	0.39
Water porosimetry				
	Total porosimetry (%)	31.1 ± 0.7	28.2 ± 0.9	7.6 ± 0.2
Mercury porosimetry				
	Total porosity (%)	30.0	25.4	6.6
	Pore threshold (µm)	0.5 and 12	0.12	0.1
	Dispersion coefficient	5.8	1.5	3.4
	Pm<0.1 (%)	3.3	50.8	33.3
	Pm<5 (%)	23	95.3	80.3
Capillary absorption				
	Capillary saturation (%)	63.1 ± 2.5	92.9 ± 2.5	55.3 ± 4.7
	C_1 Weight increase ($g.m^{-2}.s^{-½}$)	96.6 ± 5.7	66.3 ± 38.1	7.3 ± 1.2
	C_2 Wet fringe migration ($m.s^{-½}$)	0.053 ± 0.001	0.028 ± 0.018	0.011 ± 0.003

Drying				
	Drying flow at 50% R.H. ($g.m^{-2}.s^{-1}$)	-1577 ± 164	-2250 ± 218	-1315 ± 202

2.2. Salt contamination cycles

A number of 150 disk-shaped samples (diameter: 30 mm; height: 5 mm) of each stone type were submitted to immersion-drying tests in distilled water and in solutions of Na_2SO_4, NaCl and $MgSO_4$ of different concentrations: 7%, 14% and 26% in weight (Figure 3).

Figure 3: Experimental protocol and number of samples.

For NaCl and $MgSO_4$, the salt solutions were prepared by dissolving 70g, 140g and 260g of the pure salts from Fisher Scientific in 1000 ml of water for the 7%, 14% and 26% solutions respectively. For Na_2SO_4, the salt solutions were prepared by dissolving 158.73g, 317.46g and 589.57g of Na_2SO_4 decahydrate (obtained from Alfa Aesar) in 1000 ml of water for the 7%, 14% and 26% solutions respectively. Even though these concentrations were not realistic [34], they were mainly chosen in order to compare different contaminations: one corresponding to the standard EN12370 [64] which recommends a concentration of 14% of Na_2SO_4, one half lower at 7% and a stronger at 26% close to the saturation at 20°C (28%). We chose to apply the same concentration for each salt even they do not correspond to the same saturation degree as the saturation is 36% for NaCl and 26% for $MgSO_4$.

A total of 20 cycles of 24 h each were performed, consisting of 2 h immersion and 22 h of drying in boxes with silica gel at room temperature. Only for cycles 5, 10, 15 and 20, the drying phase was of 22 h + 48 h for all the samples. Solutions were renewed every 5 cycles.

After each cycle, the weight of samples was recorded with a Mettler Toledo balance of a 0.01 mg accuracy.

In addition, after 1, 5, 10 and 15 cycles, triplicate samples of each stone type, tested in water (control samples) and at each salt solution concentration were taken out for colorimetry and active infrared thermography measurements (Figure 2). Active IRT was also performed on samples of fresh stones and on the pure salts obtained by drying of saturated solution droplets on plastic slides. Although the experiment went on for 20 cycles, the samples were too degraded at that stage to perform IRT measurements. Because of painting in black the samples for the IRT measurements, these samples were not replaced in the experiments after testing. Thus, the cycles went on with a decreasing number of samples.

2.3. Colorimetry

Colour was measured with a MINOLTA CR-400 Chroma Meter using the D65 illuminant, beam of diffuse light of 8-mm diameter, 0° viewing angle geometry, specular component included and spectral response closely matching the CIE (1997) standard observer curves. Measurements are expressed following the CIE L* a* b* systems (EN 15886:2010 [65]). ΔE* is introduced as the total color change, to compare the variations before and after the tests. It is calculated from the average values of L*, a* and b* as follows: $\Delta E^* = [(\Delta L^*)^2 + (\Delta a^*)^2 + (\Delta b^*)^2]^{1/2}$. A threshold of ΔE*=3 is generally considered as the limit above which homogeneous color change is visible to the naked eye [66]. In addition, the samples were observed under a binocular magnifier after each cycle.

2.4. Active infrared thermography in the laboratory

Active IRT by pulsed thermography was conducted by means of a FLIR SC655 infrared thermography camera operating in the long-wave infrared spectral range [7.5-14 µm] and

providing images of 640 x 480 pixels. Two flash lights were placed at 45° of the sample, symmetrically along the axis of the camera, producing light of 4800 J for 5 ms (Figure 4).

Figure 4: Experimental setting of the active IRT.

The flux of photons emitted by the flash excites the sample leading to an increase of its temperature. The absorbed heat is re-emitted (mostly in the infrared spectral domain) and the corresponding thermosignal is recorded by the camera. The thermosignal depends on the physical parameters of the material: density, porosity and pore structure, specific heat, emissivity, conductivity and diffusivity, as well as on the surface properties (roughness, color) and mineralogical composition [45].

To minimize the effect of the surface aspect of the samples on the thermal response [50], laboratory samples were covered with a black high-temperature resistant paint layer with an emissivity of 0.96. All measurements were conducted in a room at a constant temperature of 21.5 °C with a relative humidity about 40%.

Images were recorded every 10 millisecond (100 Hz), and later treated and analyzed with the ThermaCAM Researcher 2.10 software (FLIR).

Thermal curves of thermal changes over time were extracted from the videos obtained. They allow giving the maximum temperature reached immediately after the flash (Tmax) (Figure 5). A ΔTmax corresponding to the increase of temperature of the sample after flash was extracted from each curve for all samples by subtracting the initial temperature of the sample to the maximum temperature reached.

Figure 5: Typical thermal curve obtained in active IRT.

3. Results and discussion

3.1 Visual and binocular magnifier observations

As early as after one cycle and furthermore other the cycles, the visual aspect of the stones changed according to the type of salt and the concentration (Figure 6). The sodium chloride and the magnesium sulfate tended to darken the stone surface while the sodium sulfate caused surface whitening due to efflorescences. Viewed under a binocular magnifier (Figure 7), the contaminated samples showed:

- A darkening with a moist aspect for $MgSO_4$ and NaCl due to transparent crystals making a glaze at the surface of the samples. While crystals filled the porosity of the surface of BJ and RS, they formed a uniform crust on SN with cubic crystals of NaCl and fan-shaped crystals of $MgSO_4$.
- A whitening with Na_2SO_4 due to efflorescences of white acicular crystals uniformly distributed on the surface.

All over the experiment, the SN samples did not show any degradation beyond colour change and efflorescence growth. Contrarily, the BJ and the RS, suffered from powdering and crack growth. The sulfates were more efficient in term of degradations than the sodium chloride.

The BJ samples showed deterioration by scaling and cracking in different conditions and cycles:

- With $MgSO_4$, disaggregation of the sample edges occurred from cycle 6 whatever the concentration and one sample broke in two parts at cycle 10;
- With Na_2SO_4 14% and 26%, scaling occurred from cycle 10 and two samples completely disaggregated at cycle 12 at 26%;

- With NaCl 14 and 26%, only a weak scaling of the edges was observed on the samples from cycle 10.

The RS samples were also damaged by the salt solutions:

- With $MgSO_4$, the samples were strongly darkened whatever the concentration. Cracks and scaling appeared from cycle 10 at 26% and cycle 15 at 14%;
- With Na_2SO_4, sanding on the edges and surface of the samples occurred all over the experiment and some samples disaggregated completely from cycle 13;
- With NaCl 26 %, scaling at edges developed from cycle 5.

These results agreed with previous studies that showed that $MgSO_4$ mainly led to crack formation, Na_2SO_4 to scaling [14,68,69] and NaCl to crystallization on the surface [4].

Figure 6: Visual evolution of samples over cycles according to salts and concentration after 1 and 20 cycles of wetting-drying in salt solutions of Na_2SO_4, $MgSO_4$ and NaCl at 7, 14 and 26% in weight.

Figure 7: View under binocular magnifier of the samples surfaces after 20 cycles in water and at 26% concentration of Na_2SO_4, $MgSO_4$ and NaCl.

3.2 Colour measurements

Samples tested in distilled water with the same number of wetting-drying cycles were used as a control. Their colour change was assessed similarly to the other samples. Colorimetry measurements on the salt-contaminated samples showed that the main parameters that changed were the L* parameter corresponding to the dark-white range and to a lesser extent

the b* parameter that measured the blue-yellow range (Figure 8). Whatever the stone and the concentration, these measurements confirmed that $NaSO_4$ was whitening the stone samples while $MgSO_4$ and NaCl were darkening them, especially $MgSO_4$ (ΔL^* up to -30).

Figure 8: Variations of L* and b* colour parameters of the Bajocian limestone (BJ), the reconstituted stone (RS) and the Sinemurian limestone (SN) after 20 cycles at different concentration of Na_2SO_4, $MgSO_4$ and NaCl solutions.

In solutions of low concentration of either salt (7%), the change of colour parameters increased with cycles while in solutions with higher concentration (14% and 26%), the maximum of change of colour parameters occurred after one cycle and then nearly stabilized over the next cycles.

Only with Na_2SO_4 did the colour parameters change with cycles and concentrations until cycle 10 then the parameters stabilized.

The white salt crust of sodium sulfate produced a mask of the stone colour, with a decrease of b*, the predominant parameter more pronounced in darker stones such as BJ. The parameter b*, also experimented an increase with the other salts, due to an optical effect of darkening.

Colour difference given by the ΔE^* parameter of samples tested in water did not exceed 2.5 for all the stones. It corresponded to a slight increase of b* for BJ and SN and of L* for RS. This change may be due to the oxidation of iron and the slight dissolution of the surface.

Values of ΔE^* of the salt contaminated samples (Figure 9) confirmed that the colour difference between stones contaminated with salts is related to the type of salts, the concentration, the number of cycles and the type of stones. From the first cycle on, and

whatever the salt, the concentration and the stone (except for SN with NaCl), ΔE* was above 3, which means that the colour change was noticeable by the naked eye.

The global colour change is less intense with NaCl (ΔE* < 10) than with $MgSO_4$ (ΔE* < 20), which is less than with Na_2SO_4 (ΔE* < 25). Overall, regarding the stones submitted to Na_2SO_4, the Bajocian limestone (BJ) experienced the most important variation, compared to the reconstituted stone (RS) and the Sinemurian limestone (SN) at the same concentration and number of cycles. Regarding the other salts, $MgSO_4$ and NaCl, BJ and RS behaved the same while SN showed an anti-correlation to salt concentration with $MgSO_4$ and a colour change visible from cycle 10 with NaCl.

Figure 9: Global colour change (ΔE*) of the Bajocian limestone (BJ), the reconstituted stone (RS) and the Sinemurian limestone (SN) after 20 cycles at different concentration of a) Na_2SO_4, b) $MgSO_4$ and c) NaCl solutions.

3.3 Weight change

The change in weight (salt uptake vs alteration) of the dried samples depended mainly on the stones and the salts. Generally, the more concentrated the solution, the higher the weight change of the sample, except for SN for which only weak weight variations (weight of the sample at the measured stage/initial dry weight) were measured (< 2%) whatever the type of salt, the number of cycles and the concentration (Figure 10). Only for NaCl 26% a weight increase of 10% was recorded after 20 cycles.

Figure 10: Normalized dry weight variation over wetting-drying cycles of the Bajocian limestone (BJ), the Sinemurian limestone (SN) and the reconstituted stone (RS) in salt solutions of Na_2SO_4, $MgSO_4$ and NaCl at different concentrations.

Weight variations of the Bajocian limestone (BJ):

- Na_2SO_4: no weight change occurred at 7%; weak change at 14% without any trend (decreased then increased to reach finally around zero after 20 cycles); at 26%, the weight increase was low after the first cycles (around 2%) and did not vary until cycle 10 from which weight increased to reach around 5% after the 20th cycle. Cycle 10 corresponded to the beginning of the disaggregation of some of the samples.
- $MgSO_4$: after the first cycle, the weight increase was high and all the more important that the solution was concentrated (+12% at 7% of $MgSO_4$; +14 % at 14 and 26% of $MgSO_4$). It maintained at this value until cycle 20 for the 26% solution. At lower concentrations, the dry weight change decreased over cycles to reach 0% at 14% $MgSO_4$ and -5% at 7% $MgSO_4$.
- NaCl: as for the $MgSO_4$, the weight increase was related to the salt concentration, relatively constant along cycles: between 2 and 4% at 7% of NaCl; between 2 and 7% at 14% of NaCl and between 5 and 15% at 26% of NaCl.

For the reconstituted stone (RS), weight variations depended also on the type of salts and tendency was similar to BJ: increase of weight only at 26% with Na_2SO_4, weight that increased from the first cycle with $MgSO_4$ and NaCl, decreased along cycles with $MgSO_4$ while it stabilized with NaCl. The weight increase for RS was a little bit higher in general: a maximum of 10% with Na_2SO_4, 18% at 26% of $MgSO_4$ and 15% at 26% of NaCl.

The porous network, and especially the pore size distribution, is widely acknowledged to control the water uptake and transport in rocks [22]. In the case of salt solutions, the porous network is thus an important factor governing salt accumulation (in terms of quantity as well as of location). Several studies have demonstrated a relationship between the total porosity and the salt uptake: the more porous the stone, the higher the salt uptake. They have also shown that the pore size distribution and the geometry of the pores play an important role: microporosity, connectivity and shape of the pores [14,20,32,70-72]. With equivalent total porosity, the higher the microporosity, the higher the salt uptake. The smallest pores with narrow pore access favour water retention in the pores and thus the salt degradations [73]. The size of the micropore threshold varies from one author to another [20].

The capillary absorption measures indirectly the connected porosity and it is often used as sustainability indicator [9] as well as the saturation coefficient [71]: stones with high porosity and fast capillary absorption but weak saturation coefficient will be salt salt resistant. Mechanical properties such as elasticity modulus [71], P waves velocity [32], tension-compression resistance [74,75] can also be used as salt weathering assessment.

Among the three stones used in this study, the SN has the lowest total porosity (7.6%, Table 1) but also low capillary properties (C_1= 7.3 $g.m^{-2}.s^{-½}$, C_2 = 0.0011 $m.s^{-½}$). The salt uptake is thus low, and salt crystallization is limited to the surface of the stone samples.

The total porosity of the BJ is the highest (31.1%), but its microporosity is also the lowest with only 3.3% of pore access smaller than 0.1 µm ($P_{m0.1}$, Table 1). That explains why RS which have a similar total porosity (28.2%) but a higher amount of microporosity ($P_{m0.1}$ = 50.8%) and a higher saturation coefficient (92.9%), has a larger salt uptake than BJ.

The salt uptake of stones depends also on the salt solution properties such as viscosity and density [14,20,70,72]. At equivalent concentrations, NaCl has the lowest viscosity (1528 µPa.s at 29.22 weight % at 25°C [76]), Na_2SO_4 an intermediate value (2243 µPa.s at 26

weight % at 30°C [77]) while $MgSO_4$ has the highest (7270 µPa.s at 33.5 weight % at 20°C [14]). Furthermore, the viscosity of salts increases with the concentration (i.e. Na_2SO_4 at 5 mass % 1035 µPa.s, 1545 µPa.s at 15 mass % and 2243 µPa.s at 26 mass % [77].

The increase of viscosity slows down the capillary absorption and as a consequence, it modifies the salt crystallization and their location [16]. With lower transfer properties, the evaporation occurs faster than the supply of the solution by capillarity from the inside of the stone, and precipitation takes place under the stone surface [14,78]. High concentrations can also favour pore clogging, which reduces the drying, the transport of salts through the porous network and thus enables the growth of subflorescences [79]. The drying of high-concentration solutions is also decreased because of smaller difference of vapor pressure between the material and the surroundings [80].

High concentrations are not necessarily indispensable to observe decay. The alternation of absorption-drying with low concentrated solutions can allow a larger accumulation of salts and thus the decay of the material [68,81,82].

3.4 Active infrared thermography

By painting the samples in black after a drying to a constant weight and by performing the IRT measurements always in the same conditions, the thermal response depends only on the chemical composition of the surface, its roughness and porosity.

Thermal signature of fresh stones and pure salts

The thermal responses of the fresh stones, corresponding to the increase of temperature due to the flash, were different according to the type of stone (Table 2). The ΔTmax of the BJ limestone was quite low (18 °C) compared to SN and RS for which the ΔTmax was close,

respectively of 33 and 29 °C. The emissivity of the samples were constant and equal to the one of the black painting (0.96), thus the energy deposited at the surface (Q) did not vary and the ΔTmax depended mainly on the effusivity variation (b) of the surface (Eq. 1).

$$\Delta T_{max} = \frac{Q}{b\sqrt{\pi t}} \qquad \text{(Eq. 1)}$$

The composition and the porosity of the materials could explain the different thermal behaviours of the stones because effusivity is related to the bulk density (ρ), the conductivity (C) and the heat capacity (k) of the material (Eq. 2).

$$b = \sqrt{\rho C k} \qquad \text{(Eq. 2)}$$

The BJ limestone is made mainly of calcite and its porosity is high (31.1%) while the SN limestone is rich in silica and has a low porosity (7.6%). The RS stone has a high porosity but a high content of silica. Regarding the values of the literature, the effusivity of limestone is around 2300 J K^{-1} m^{-2} $s^{-1/2}$ while the effusivity of sand is 1500 J K^{-1} m^{-2} $s^{-1/2}$ [83] thus the presence of silica will increase the thermal response since a low effusivity means that the stone release the heat slowly or in a lesser extent. On the contrary, the increase of porosity will reduce the thermal response due to the air effusivity within the pores.

The thermal response of the salts tested separately was also different according to the type of salts: $MgSO_4$ and Na_2SO_4 had similar ΔTmax around 27°C while the ΔTmax of NaCl was lower, around 10°C (Table 2).

Table 2: Values of ΔTmax of the fresh stones and the salts alone.

	BJ	RS	SN	Na_2SO4	$MgSO_4$	NaCl
ΔTmax (°C)	18.4 ± 0.5	28.9 ± 0.4	33.2 ± 1.1	27.0	27.6 ± 2.4	9.8 ± 1.7

According to table 2, if the pulse thermography only records the signature of the surface of the material (less than 100 μm), the thermal response (ΔTmax) of NaCl that covers the

surface with a layer of glossy cubic crystals reflecting the radiation, should decrease for all the contaminated stones. On the other hand, the ΔTmax due to sulfate crystallization should increase for BJ, decrease slightly for SN and should not change for RS.

Regarding the evolution of ΔTmax (Figure 11) and the corresponding IRT images (Figure 12), the contaminated stones did not behave similarly to active IRT according to the type of salt, the concentration of the solution and the number of wetting-drying cycles as expected.

We could distinguish BJ and RS behaviour, the most porous materials from SN, the less porous limestone.

SN,is a limestone with low and microporous porosity associated to weak capillary transfer prevent the stone from taking up salt and thus very limited crystallization occurs inside the porous network. Salts crystallize at the surface without modifying the porous network. The thermal response of the salt-laden stone is thus very similar to the one of the pure salt.

However, thanks to the thermal images at Tmax (Figure 12), slight variations could be enhanced.

After one cycle with Na_2SO_4 at 7% and NaCl at each concentration, ΔTmax was close the thermal signature of the stone (Cycle 0). This was mainly due to the weak amount of efflorescences at the surface of the samples at that stage (Figure 6).

For the other concentrations and salts, the thermal response over the cycles was nearly constant and close to the thermal signature of the pure salt due to the covering of the surfaces by salts. In the case of sulfates, the ΔTmax was lower than the salt signature. This could be explained by the roughness of efflorescences.

BJ and RS have high porosity and high capillary transfer that enable the salt uptake.

For these stones, the thermal response was similar and depended mainly on the type of salts and the number of wetting-drying cycles: from one to ten cycles and after ten cycles.

- Type of salt

From the first cycle, the ΔTmax recorded was higher with Na_2SO_4 than with $MgSO_4$ even though the sulfates alone had similar thermal signature. The salt uptake at the first cycles was higher in the case of $MgSO_4$ (Figure 9) but tended to decrease with cycles, especially for high concentrations. On the contrary, the salt uptake of Na_2SO_4 was lower from the first cycles but increased along the test. The thermal response of stones contaminated with NaCl was low, in agreement with the low thermal response of this salt.

The differences in thermal response of the type of salt were related to the salt uptake and to the different locations of crystallization, inside or at the surface of the porous network. For $MgSO_4$, crystals did not cover all the surface of the stones while for Na_2SO_4, acicular crystals covered the whole surface. During wetting-drying cycles with salt solutions, some salts that crystallize during drying are once again dissolved and thus are mobilized during the next wetting phase. The crystallization of salts inside the porous network induces stresses on the porous matrix that enlarge the pores [14]. There is a competition between filling of porosity with crystals and widening of the pores that depends on the salt solution and the stone properties.

From one to ten cycles, ΔTmax increased with the concentration of the solution and the number of cycles. This was especially noticeable for the sulfate contaminations. When contaminated with NaCl, the thermal response of BJ and RS remained close to the fresh stone signature.

Along the wetting-drying cycles, the crystallization of salts on the surface and inside the pores, called pore clogging, replacing air by crystals, tended to increase the thermal response of the stone.

From cycle 10 the thermal response decreased to a value close to the salt signature whatever the concentration of the solution and remained constant with the number of cycle. That corresponded to the beginning of sanding of the samples. The opening of the porosity decreased the thermal response. When contaminated with NaCl, the ΔTmax was close to the corresponding salt signature (9.8 °C).

On stones with low porosity and weak capillary kinetics that are sensitive to salt efflorescences growth, the active IRT by pulse will allow to detect the type of salts according to the thermal signature of salts: sulfate could be distinguished from sodium chloride that have contrasting thermal signature. That could be useful especially on architectural parts that are hardly accessible.

On stones with high porosity and high capillary transfer, the thermal signature will be related to the concentration of the solution because of the filling of the porosity by salts over the cycles. However, it will work especially with salts that crystallize in the pores like sulfates and less with salts that forms a varnish on the surface like chloride.

Figure 11: Temperature increase after flash (ΔTmax) of the three building stones recorded with active infrared thermography after cycles of wetting-drying contamination with different salt solutions (the dot lines indicate the thermal signature of the corresponding salt).

Figure 12: Thermal images at Tmax of rock samples according to salts and concentration after 1 and 15 cycles of wetting-drying in salt solutions of Na_2SO_4, $MgSO_4$ and NaCl at 7, 14 and 26% in weight.

4. Conclusions

The infrared thermography results in a promising tool to detect the presence of salts in stones as well as their composition and concentration. Different experiments were carried out in laboratory to test the suitability of the technique. The main results revealed that:

- The difference in composition, roughness and porosity leads to different initial thermal signature when tested in pulse active IRT as observed on fresh materials as well as on pure salts;
- When porosity of stones is high (BJ, RS), the thermal response to heating (ΔTmax) is related to salt concentration: ΔTmax increases with salt uptake due to pore clogging as long as the samples are not deteriorated;
- When the stone starts to disaggregate, the increase of porosity and the crystallization of salts combine and the thermal signature is nearly constant and close to the one of salts;
- When porosity is low (SN), salts do not enter the porous network and the ΔTmax corresponds to salt thermal signature of the efflorescences with no relation with the salt solution concentration.

Active IRT is a NDT adapted to identify and quantify salts within building stones but it is necessary to use it during the first states of accumulation. Further tests with longer heating to have deeper response of the stone and tests in the field on a well-characterized wall would be necessary.

Acknowledgements

This study was partly funded by the Hybriprotech grant as part of the INTERREG IV programme and the starting grant TRANSELS financed by the University of Reims Champagne–Ardenne. The authors warmly thank Brother Xavier for permitting work and sample collection in the Orval Abbey and A. Thomachot for her editing assistance.

Conflict of Interest

The authors declare that they have no conflict of interest.

References

[1] Oguchi C.T. and Matsukura Y (2000) Spatial distribution of salt efflorescence on brick walls in the Shimoren Kiln, central Japan. Ann. Rep. Inst. Geosci., Univ. Tsukuba, 26:25-29

[2] Sabbioni C (1995) Contribution of atmospheric deposition to the formation of damage layers, The Science of the Total Environment. 167:49-55

[3] Gibeaux S, Martinez-Garrido MI, Vazquez P, Thomachot-Schneider C, Fort R (2018) Wireless environmental monitoring and portable techniques for decay risk analysis at St Joseph chapel (Reims, France), Sensors and Actuators Actuators A: Physical, 272:102-113.

[4] Morillas H, Vazquez P, Maguregui M, Marcaida I, Silva L.F.O. (2018) Composition and porosity study of original and restoration materials included in a coastal historical construction. Construction and Building Materials, 178, pp. 384-392.

[5] Anson-Cartwright T, Bourguignon E, Bromblet P, et al. (2008) ICOMOS-ISCS: Illustrated glossary on stone deterioration patterns-Glossaire illustré sur les formes d'altération de la pierre.

[6] Shahidzadeh-Bonn N, Desarnaud J, Bertrand F, et al. (2010) Damage in porous media due to salt crystallization. Phys Rev E - Stat Nonlinear Soft Matter Phys. doi: 10.1103/PhysRevE.81.066110

[7] Flatt R, Aly N, Caruso F, Derluyn H, Desarnaud J, Lubelli B, Espinosa RM, Pel L, Rodriguez-Navarro C, Scherer GW, Shahidzadeh N, Steiger M (2017) Predicting salt

damage in practice: a theoretical insight into laboratory tests. RILEM Tech Lett 2:108–118

[8] Arnold B (1983) Determination of mineral salts from monuments, Studies in Conservation, 29:129-138

[9] Goudie AS, Viles HA (1995) The nature and pattern of debris liberation by salt weathering: a laboratory study. Earth Surf Proc Land 20(5):437–449. https://doi.org/10. 1002/esp.3290200505

[10] Winkler EM (1966) Important agents of weathering for building and monumental stone. Eng Geol 1:381–400. doi: 10.1016/0013-7952(66)90003-2

[11] Saiz-Jimenez C (1993) Deposition of airborne organic pollutants on historic buildings. Atmospheric Environement. Part B Urban Atmosphere 27:1:77-85

[12] Goudie A, Cooke R, Evans I (1970) Experimental investigation of rock weathering by salts. Area 2(4):42–48

[13] Yu S and Oguchi CT (2009) Complex relationships between salt type and rock properties in a durability experiment of multiple salt-rock treatments. Earth Surf Process Landf 34:2096–2110. doi: 10.1002/esp.1904

[14] Ruiz-Agudo E, Mees F, Jacobs P, Rodriguez-Navarro C (2007) The role of saline solution properties on porous limestone salt weathering by magnesium and sodium sulfates. Environ Geol 52(2):269–281. https://doi.org/10. 1007/s00254-006-0476-x

[15] Rodriguez-Navarro C and Doehne E (1999) Salt weathering: influence of evaporation rate, supersaturation and crystallization pattern. Earth Surf. Process. Landforms 24, 191-209

[16] Lubelli B, Cnudde V, Diaz-Goncalves T, Franzoni E, van Hees R. P. J, Ioannou I, Menendez B, Nunes C, Siedel H, Stefanidou M, Verges-Belmin V, Viles H (2018) Towards a more effective and reliable salt crystallization test for porous building materials: state of the art Materials and Structures 51:55 https://doi.org/10.1617/s11527-018-1180-5

[17] Gomez-Heras M, Fort R. (2007). Patterns of halite (NaCl) crystallisation in building stone conditioned by laboratory heating regimes. Environmental geology, 52(2), 259-267.

[18] Jeannette D (1997) Importance of the Pore Structures During the Weathering Process of Stones in Monuments. In: Soils and sediments. Springer, pp 177–190

[19] Beck K, Al-Mukhtar M, Rozenbaum O, Rautureau M (2003) Characterization, water transfer properties and deterioration in tuffeau: Building material in the Loire valley-France. Build Environ 38:1151–1162. doi: 10.1016/S0360-1323(03)00074-X

[20] Yu S and Oguchi CT (2010) Role of pore size distribution in salt uptake, damage, and predicting salt susceptibility of eight types of Japanese building stones. Eng Geol 115:226–236. doi: 10.1016/j.enggeo.2009.05.007

[21] Thomachot-Schneider C, Gommeaux M, Fronteau G, et al. (2011) A comparison of the properties and salt weathering susceptibility of natural and reconstituted stones of the Orval Abbey (Belgium). Environ Earth Sci 63:1447–1461. doi: 10.1007/s12665-010-0743-8

[22] Vos BH (1976) Water absorption and drying of materials. In: Rossi-Manaresi, R. (Ed.), The Conservation of Stone I, Centro per la Conservazione delle Sculture All'Apperto, Bologna, pp. 679–694.

[23] Wellman HW, Wilson AT (1965) Salt weathering, a neglected geological erosive agent in coastal and arid environments. Nature 205, 1097–1098.

[24] Flatt RJ (2002) Salt damage in porous materials: How high supersaturations are generated. J Cryst Growth 242:435–454. doi: 10.1016/S0022-0248(02)01429-X

[25] Scherer GW (2006) Internal stress and cracking in stone and masonry. In: KONSTA-GDOUTOS MS (ed) Measuring, Monitoring and Modeling Concrete Properties. Springer Netherlands, pp 633–641

[26] Steiger M (2005) Crystal growth in porous materials—II: influence of crystal size on the crystallization pressure. Journal of Cryst Growth 282, 470–481.

[27] Fitzner B (1988) Porosity properties of naturally or artificially weathered sandstone. In: Ciabach J (Ed.), Proceedings of the 6th International Congress on Deterioration and Conservation of Stone, Toruń, Poland, pp. 236–245.

[28] Zehnder K, Arnold A (1989) Crystal growth in salt efflorescence. Journal of Crystal Growth 97, 513–521.

[29] Ordóñez S, Fort R, García del Cura M.A. (1997) Pore size distribution and the durability of a porous limestone. Quarterly Journal of Engineering Geology 30, 221–230.

[30] Punuru A.R. Chowdhury A.N. Kulshreshtha N.P. Gauri K.L. (1990) Control of porosity on durability of limestone at the Great Sphinx, Egypt. Environmental Geology and Water Science 15, 225–232.

[31] Rossi-Manaresi R & Tucci A (1991) Pore structure and the disruptive or cementing effect of salt crystallization in various types of stone. Studies in Conservation 36, 53–58.

[32] Benavente D, García del Cura MA, Fort R, Ordóñez S (2004) Durability estimation of porous building stones from pore structure and strength. Engineering Geology 74, 113–127.

[33] Ruiz-Agudo E, Lubelli B, Sawdy A, van Hees R, Price C, Rodriguez-Navarro C (2011) An integrated methodology for salt damage assessment and remediation: the case of San Jeronimo Monastery (Granada, Spain). Environ Earth Sci 63:1475–1486

[34] Modestou S, Theodoridou M, Ioannou I (2015) Micro-destructive mapping of the salt crystallization front in limestone. Engineering Geology 193:337–347

[35] Mercuri F, Orazi N, Zammit U, et al. (2012) Thermographic analysis of cultural heritage: recent applications and perspectives. Thermogr Cult Herit 9:84–89.

[36] Danese M, Sileo M, Masini N (2018). Geophysical Methods and Spatial Information for the Analysis of Decaying Frescoes. Surveys in Geophysics, 1-18, doi: 10.1007/s10712-018-9484-0

[37] Lerma C, Mas Á, Gil E, et al. (2014) Pathology of building materials in historic buildings. Relationship between laboratory testing and infrared thermography. Mater Constr 64:e009.

[38] Moropoulou A, Avdelidis N, Ekaterini M, Delegou E, Alexakis E and Keramidas V (2018) Multispectral Applications of Infrared Thermography in the Diagnosis and Protection of Built Cultural Heritage, Applied Sciences 8(2):284

[39] Thomachot-Schneider C, Vazquez P, Lelarge N, et al. (2014) Thermal behaviour of building stones submitted to salt solutions. SWBSS 2014, Brussels,

[40] Grinzato E, Vavilov V, Kauppinen T (1998) Quantitative infrared thermography in buildings. Energy Build 29:1–9.

[41] Grinzato E, Bressan C, Marinetti S, et al. (2002) Monitoring of the Scrovegni Chapel by IR thermography: Giotto at infrared. Infrared Phys Technol 43:165–169. doi: 10.1016/S1350-4495(02)00136-6

[42] Bodnar JL, Nicolas JL, Mouhoubi K, et al. (2013) Characterization of an inclusion of plastazote located in an academic fresco by photothermal thermography. Int J Thermophys 34:1633–1637. doi: 10.1007/s10765-012-1335-5

[43] Masini N, Montano V., Ponzo F., Di Cesare A., Geraldi E., Gizzi F., Leucci G., Sileo M. (2015) Multiscale and multisensor approach for the structural diagnosis of ancient buildings: the case of the" Domus of the Silver Wedding" in Pompei. TECHNART 2015 Non-destructive and microanalytical techniques in art and cultural heritage. At: Catania, Italy

[44] Matera L., Persico R., Geraldi E., Sileo M., Piro S. (2016) GPR and IRT tests in two historical buildings in Gravina in Puglia. Geoscientific instrumentation, methods and data systems discussions, 1-19

[45] Kylili A, Fokaides PA, Christou P, Kalogirou SA (2014) Infrared thermography (IRT) applications for building diagnostics: A review. Applied Energy 134:531–549

[46] Moropoulou A, Koui M, Avdelidis NP (2000) Infrared thermography as an NDT tool in the evaluation of materials and techniques for the protection of historic monuments. Insight Non-Destr Test Cond Monit 42:379–383.

[47] Ludwig N, Rosina E, Sansonetti A (2017), Evaluation and monitoring of water diffusion into stone porous materials by means of innovative IR thermography techniques, Measurement dx.doi.org/10.1016/j.measurement.2017.09.002

[48] Edis E, Flores-Colen I, de Brito J (2015) Quasi-quantitative infrared thermographic detection of moisture variation in facades with adhered ceramic cladding using principal component analysis. Build Environ 94:97–108. doi: 10.1016/j.buildenv.2015.07.027

[49] Avdelidis NP, Moropoulou A (2004) Applications of infrared thermography for the investigation of historic structures. J Cult Herit 5:119–127. doi: 10.1016/j.culher.2003.07.002

[50] Avdelidis NP, Moropoulou A, Theoulakis P (2003a) Detection of water deposits and movement in porous materials by infrared imaging. Infrared Phys Technol 44:183–190. doi: 10.1016/S1350-4495(02)00212-8

[51] Gomez-Heras M, Garcia Morales S, Fort, R. (2013). Integración de datos de termografía de infrarrojos y otras técnicas no destructivas en detección de humedades y sales. Jornada de Técnicas de Reparación y Conservación del Patrimonio, 11.

[52] Gómez-Heras M, McAllister D, Flechoso M.A.G., González R.F., Morales S.G. (2014). Ejemplos de análisis cuantitativo de imágenes de infrarrojos obtenidas por termografía activa para la detección de patologías de humedades. In Congreso Latinoamericano sobre patología de la construcción, tecnología de la rehabilitación y gestión del patrimonio: REHABEND 2014, Santander (España), 1-4 de abril de 2014 (pp. 461-468). Universidad de Cantabria.

[53] Bodnar JL, Candoré JC, Nicolas JL, et al. (2012) Stimulated infrared thermography applied to help restoring mural paintings. NDT E Int 49:40–46. doi: 10.1016/j.ndteint.2012.03.007

[54] Schwarz K, Heitkötter Heil J, Marschner B, Stumpe B (2018) The potential of active and passive infrared thermography for identifying dynamics of soil moisture and microbial activity at high spatial and temporal resolution, Geoderma 327:119-129

[55] Vázquez P, Thomachot-Schneider C, Mouhoubi K, et al. (2015) Infrared thermography monitoring of the NaCl crystallisation process. Infrared Phys Technol 71:198–207. doi: 10.1016/j.infrared.2015.03.013

[56] Vázquez P., Thomachot-Schneider C., Mouhoubi K., Bodnar, J. L., Avdelidis, N. P., Charles, D., & Benavente, D. (2018). Sodium sulfate crystallisation monitoring using IR thermography. Infrared Physics & Technology, 89, 231-241

[57] Wiggenhauser H (2002) Active IR-applications in civil engineering. Infrared Phys Technol 43:233–238. doi: 10.1016/S1350-4495(02)00145-7

[58] Lerma C and Barreira E (2018) A discussion concerning active infrared thermography in the evaluation of buildings air infiltration (https://doi.org/10.1016/j.enbuild.2018.02.050

[59] Theodorakeas P, Cheilakou E, Ftikou E, Koui M (2015) Passive and active infrared thermography: an overview of applications for the inspection of mosaic structures, 33rd UIT (Italian union of thermo-fluid-dynamics) heat transfer conference. J. Phys.: Conf. Ser 655

[60] Balgeas D, Maldague X, Burleigh D, Vavilov VP, Oswald-Tranta B, Roche J-M, Pradere C, Carlomagno GM (2016) Thermal (IR) and Other NDT Techniques for Improved Material Inspection, J Nodestruct Eval 35:18

[61] Maldague X (2002) Introduction to NDT by Active Infrared Thermography, Materials Evaluation, 6:9:1060 -1073

[62] Fujimaki T, Osawa Y, Oguchi CT, et al. (2011) Salt weathering susceptibility of natural limestone and reconstituted stone used in the Orval Abbey, Belgium. SWBSS2011 Limassol, Cyprus, pp 19–22

[63] Gommeaux M, Thomachot-Schneider C, Fronteau G, et al. (2014) Salt weathering processes of reconstituted stone used in the Orval Abbey (Belgium). SWBSS 2014 Brussels, pp 521–524

[64] EN 12370:1999. Determination of resistance to salt crystallization, Natural stone test methods

[65] EN 15886:2010. Conservation of cultural property. Test methods. Colour measurement of surfaces

[66] Grossi CM, Alonso FJ, Esbert RM, Rojo A (2007) Effect of laser cleaning on granite color. Color Res Appl 32:152–159. doi: 10.1002/col.20299

[67] Avdelidis NP, Moropoulou A. (2003b) Emissivity considerations in building next term thermography. Energy Build, 35:663–7.

[68] Balboni E, Espinosa-Marzal RM, Doehne E, Scherer GW (2010) Can drying and re-wetting of magnesium sulfate salts lead to damage of stone? Environ Earth Sci 63(7–8):1463–1473. https://doi.org/10.1007/s12665-010- 0774-1

[69] Espinosa-Marzal RM, Scherer GW (2011) Mechanisms of damage by salt. Geol Soc Lond Spec Publ 331(1):61–77. doi:10.1144/sp331.5

[70] Hall C, Hoff WD, Taylor SC, Wilson MA, Beom-Gi Yoon, Reinhardt HW., Sosoro M, Meredith P, Donald AM (1995) Water anomaly in capillary liquid absorption by cement-based materials. Journal of Materials Science Letter 14, 1178–1181.

[71] Goudie AS (1999) Experimental salt weathering of limestones in relation to rock properties. Earth Surf Proc Land 24:175–724

[72] Benavente D, García del Cura MA, Fort R, Ordóñez S (2001) Quantification of salt weathering in porous stones using an experimental continous partial immersion method. Engineering Geology 59:313-325

[73] Kozlowski R, Magiera J, Weber J and Haber J (1990) Decay and conservation of Pinczow porous limestone. Part 1. Lithology and weathering. Studies in Conservation35:205–21

[74] Angeli M, Bigas J-P, Benavente D, et al. (2007) Salt crystallization in pores: Quantification and estimation of damage. Environ Geol 52:187–195. doi: 10.1007/s00254-006-0509-5

[75] Benavente D, Cueto N, Martinez-Martinez J, García del Cura M A, Canaveras J C (2007) The influence of petrophysical properties on the salt weathering of porous building rocks. Environ Geol 52:215–224 DOI 10.1007/s00254-006-0475-y

[76] Abdulagatov IM, Zeinalovab A, Azizov ND (2005) Viscosity of aqueous Na2SO4 solutions at temperatures from 298 to 573 K and at pressures up to 40 MPa, Fluid Phase Equilibria 227:57–70

[77] Aleksandrov AA, Dzhuraeva EV and Utenkov VF (2012) Viscosity of Aqueous Solutions of Sodium Chloride, High Temperature, 50:3: 354–358.

[78] Angeli M, Herbert R, Menendez B, David C, Bigas J-P (2010) Influence of temperature and salt concentration on the salt weathering of a sedimentary stone with sodium sulfate. Eng Geol 115(3–4):193–199. https://doi.org/10. 1016/j.enggeo.2009.06.001

[79] Godts S, Hendrickx R, De Clercq H (2014) The crystallization behavior of sodium magnesium sulfate in limestone. In: De Clercq H (ed) Proceedings of the third international conference on salt weathering of buildings and stone sculptures (SWBSS 2014), Aedificatio Publishers, Brussels, pp 167–182

[80] Gonçalves TD (2007) Salt crystallisation in plastered or rendered walls. Ph.D. dissertation, Instituto Superior Tecnico da Universidade Te´cnica de Lisboa

[81] Wijffels T, Lubelli B (2006) Development of a new accelerated salt crystallization test. Heron 51(1):63–79

[82] Lubelli B (2006) Sodium chloride damage to porous building materials. PhD dissertation, Delft University of Technology

[83] De Vriendt A.B. (1984) La transmission de la chaleur Volume 1, Généralités, la conduction Tome 1, Généralités, la conduction / Chicoutimi (Québec) : G. Morin , DL

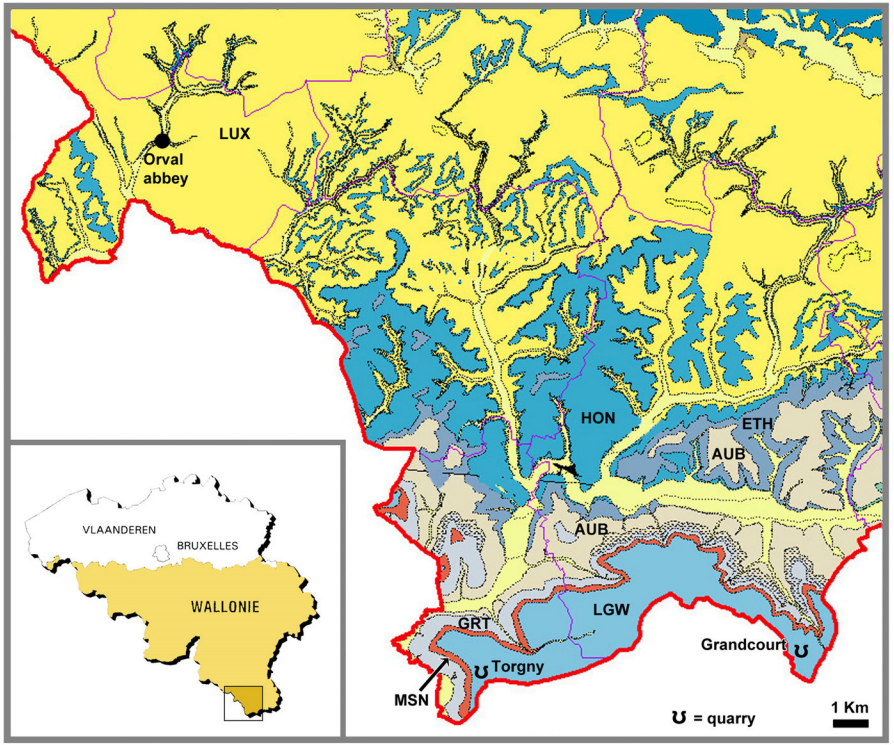

Period	Age	Formations in southern Wallonia	
			176 Ma
MIDDLE JURASSIC	Bajocian	Longwy (LGW)	
			183 Ma
	Aalenian	Mont-Saint-Martin (MSN)	
			187 Ma
LOWER JURASSIC	Toarcian	Grandcourt (GRT)	
			193 Ma
	Pliensbachian	Aubange (AUB)	
		Ethe (ETH)	
		Hondelange (HON)	
			198 Ma
	Sinemurian	Luxembourg (LUX)	
			204 Ma

a)

b)

c)

d)

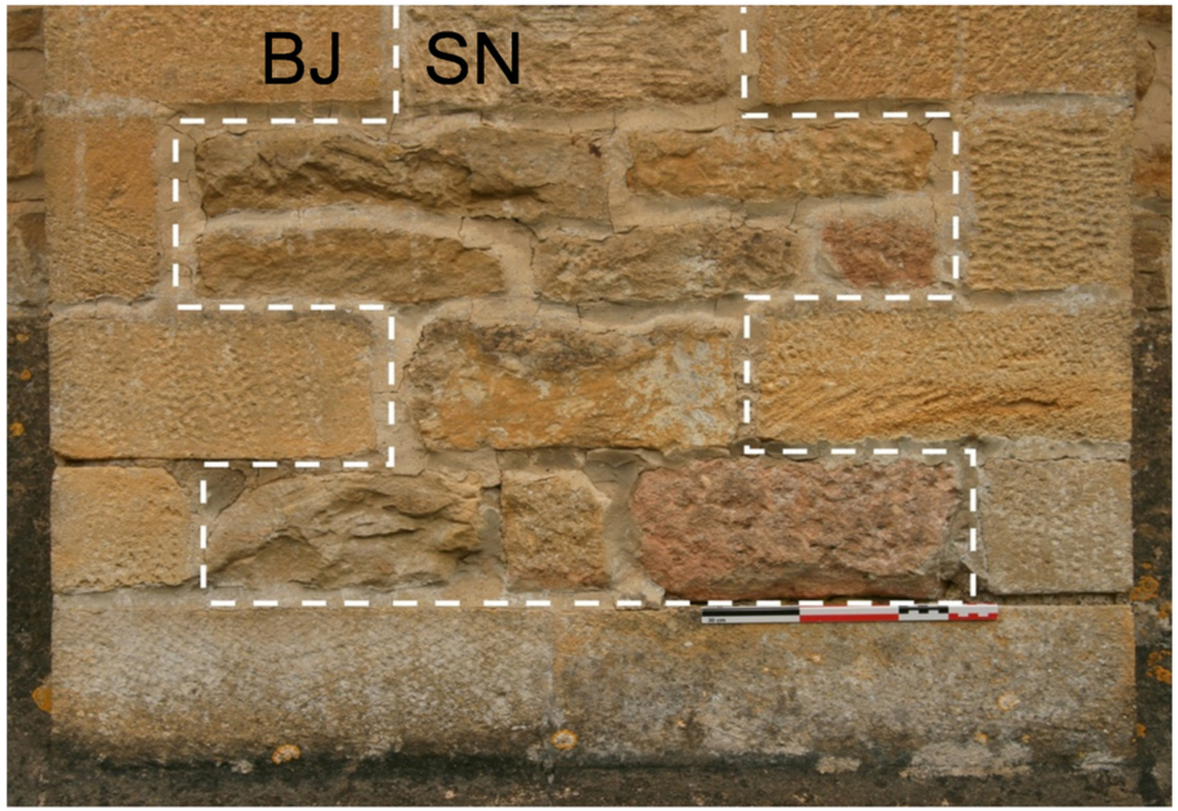

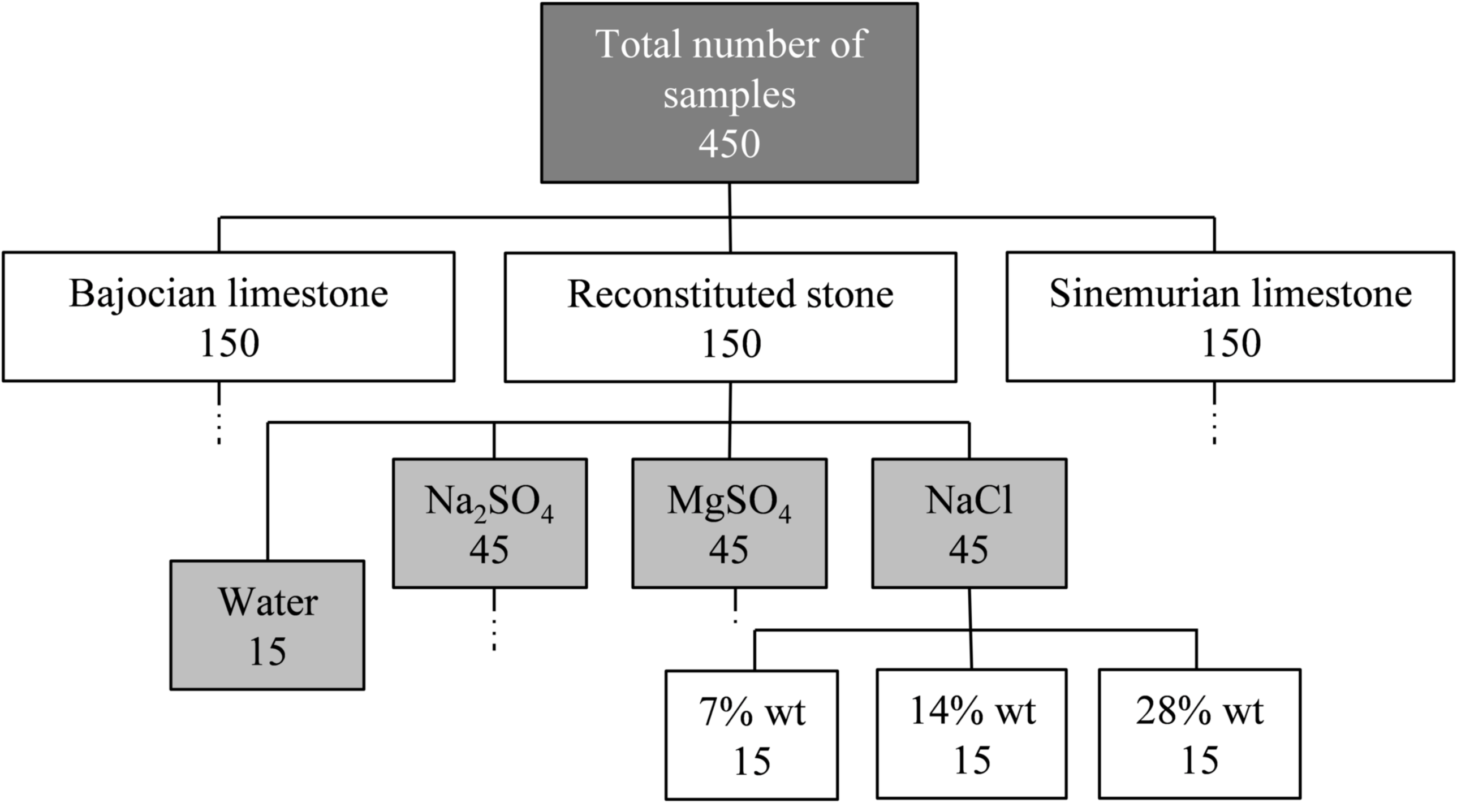
Total number of samples 450
Bajocian limestone 150
Reconstituted stone 150
Sinemurian limestone 150
Water 15
Na_2SO_4 45
$MgSO_4$ 45
NaCl 45
7% wt 15
14% wt 15
28% wt 15

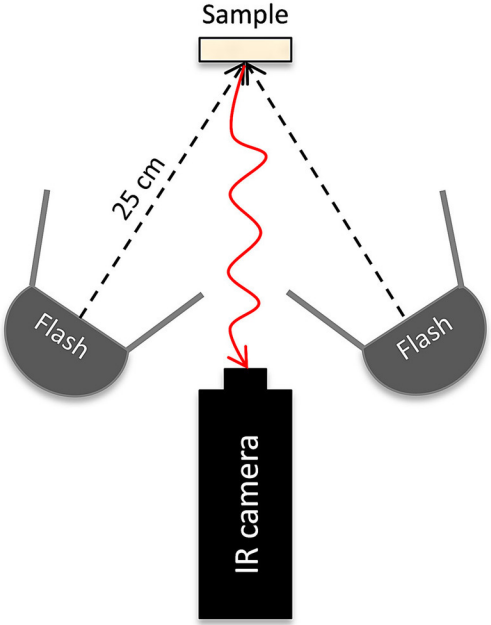
Sample
25 cm
Flash
Flash
IR camera

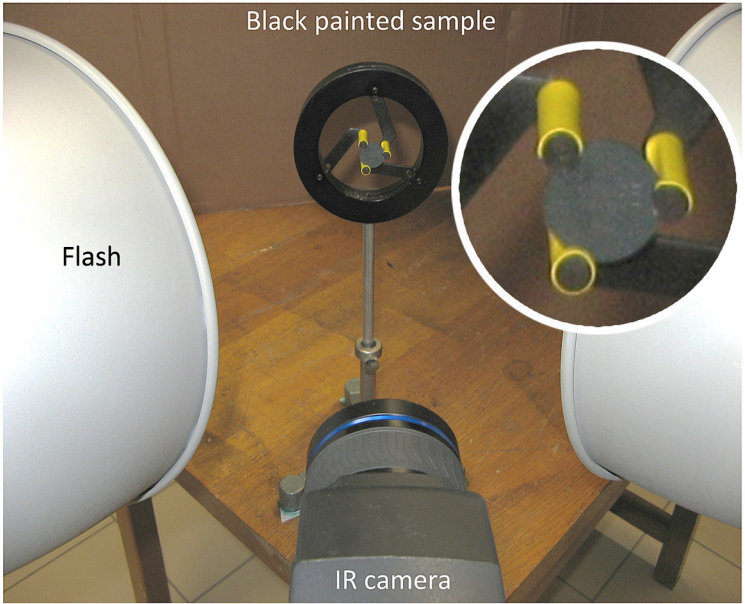
Black painted sample
Flash
IR camera

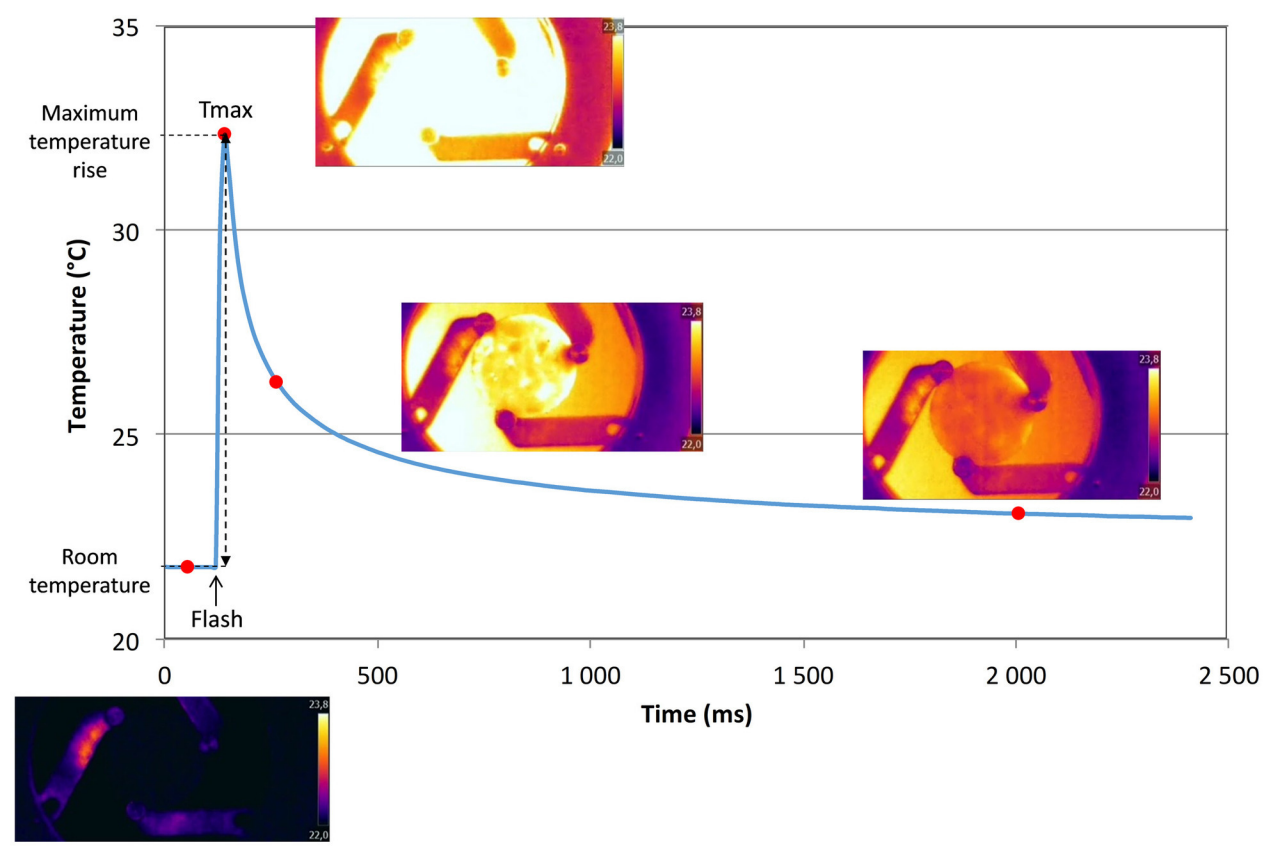
35
30
25
20
Temperature (°C)
Maximum temperature rise
Tmax
Room temperature
Flash
0
500
1 000
1 500
2 000
2 500
Time (ms)
23,8
22,0

BJ

RS

SN

7% 14% 26% 7% 14% 26% 7% 14% 26%

Na_2SO_4 Cycle 1

Cycle 20

$MgSO_4$ Cycle 1

Cycle 20

NaCl Cycle 1

Cycle 20

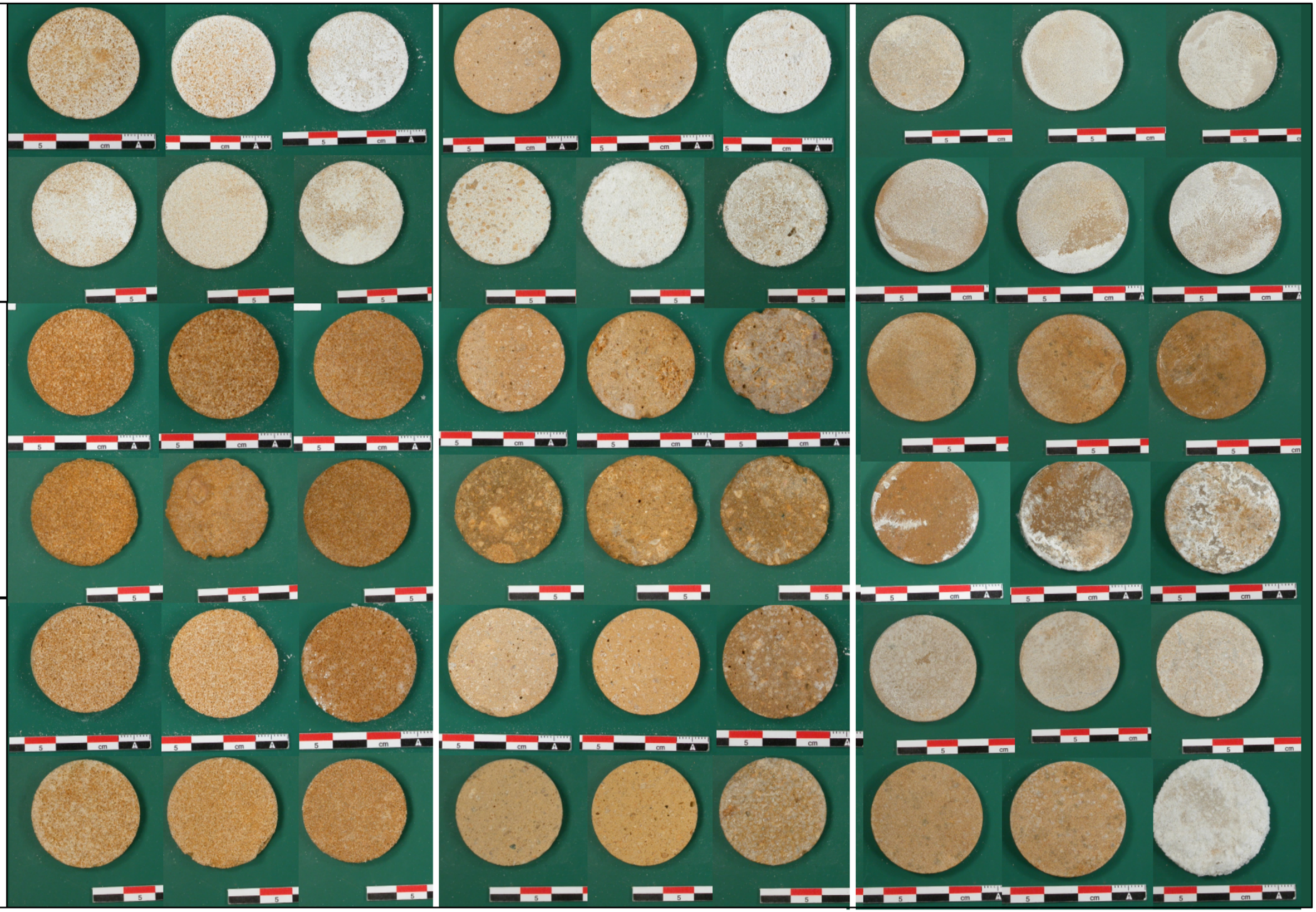

RS

BJ

SN

Water

Na_2SO_4 – 26%

$MgSO_4$ – 26%

NaCl – 26%

1 mm

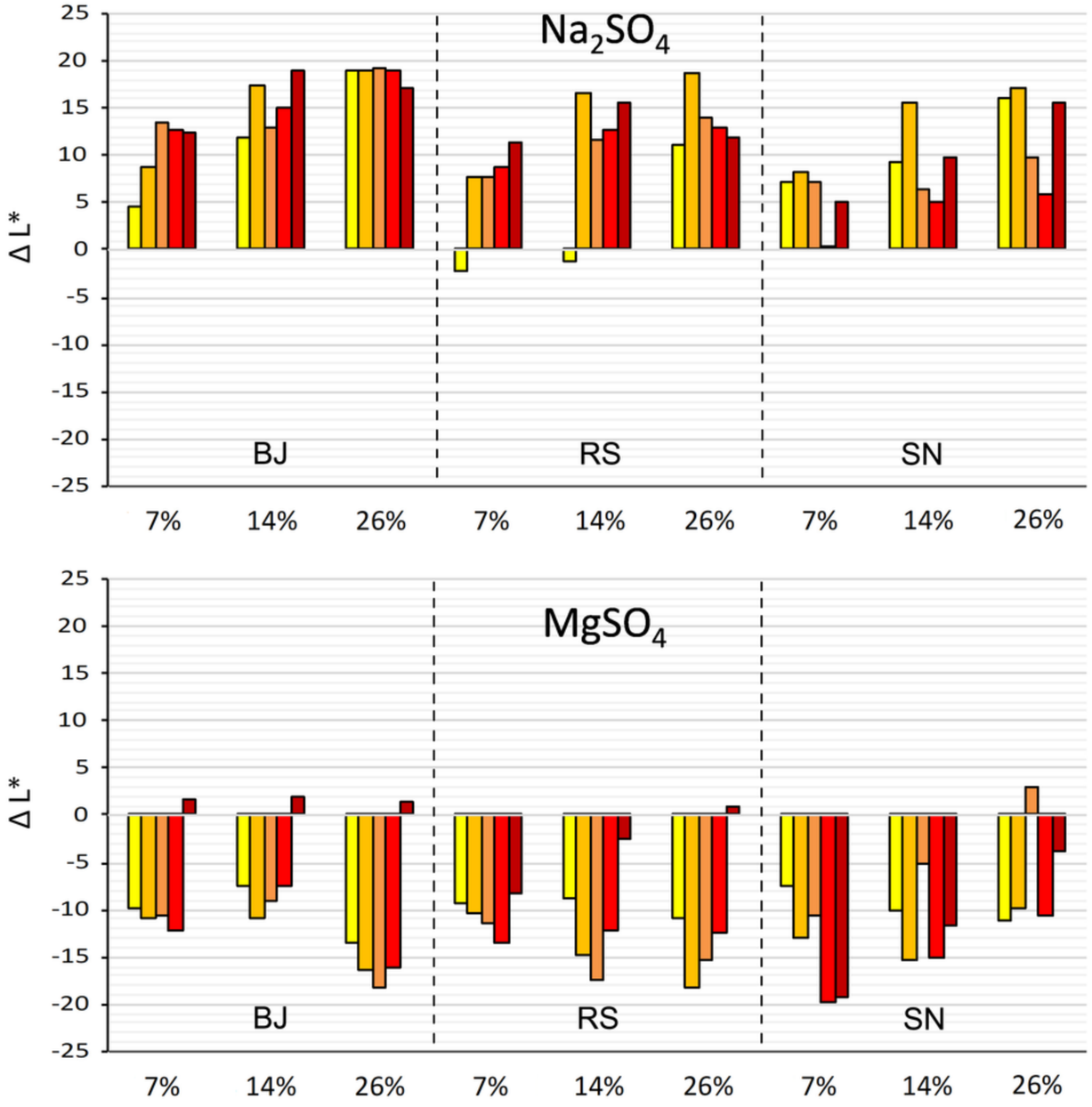

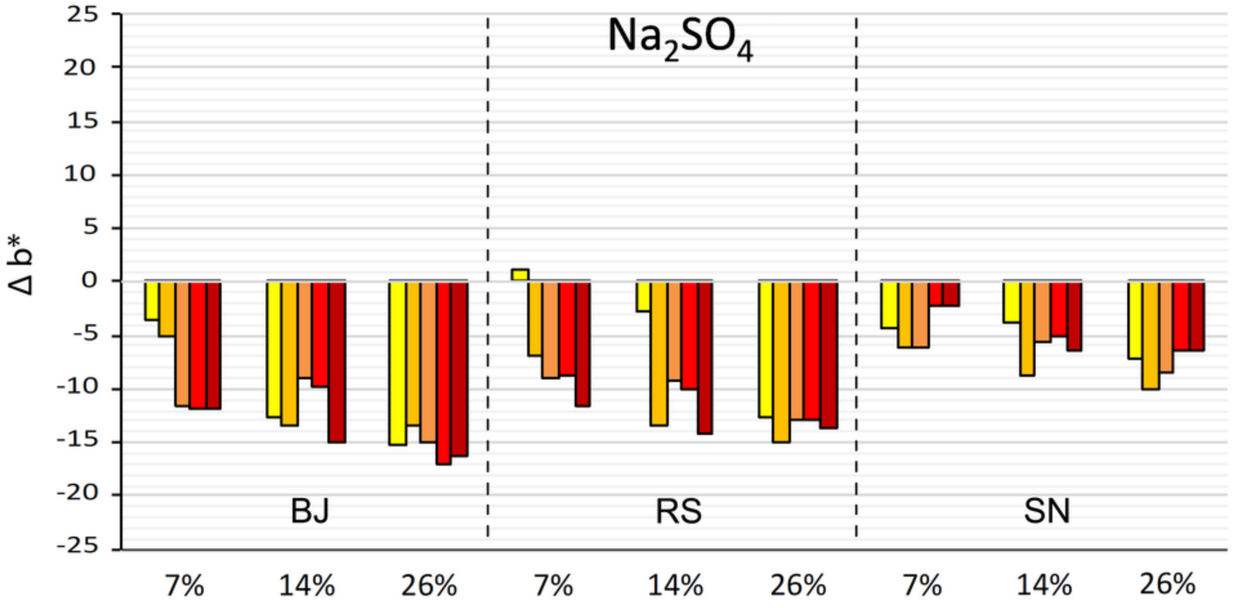

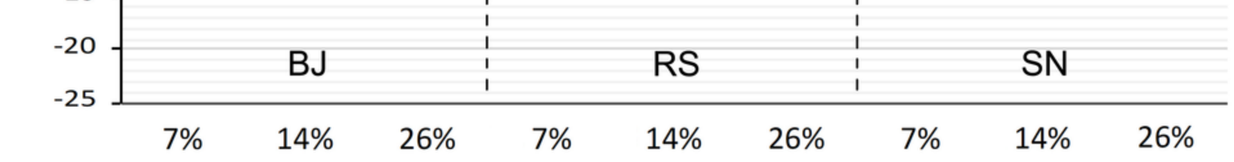

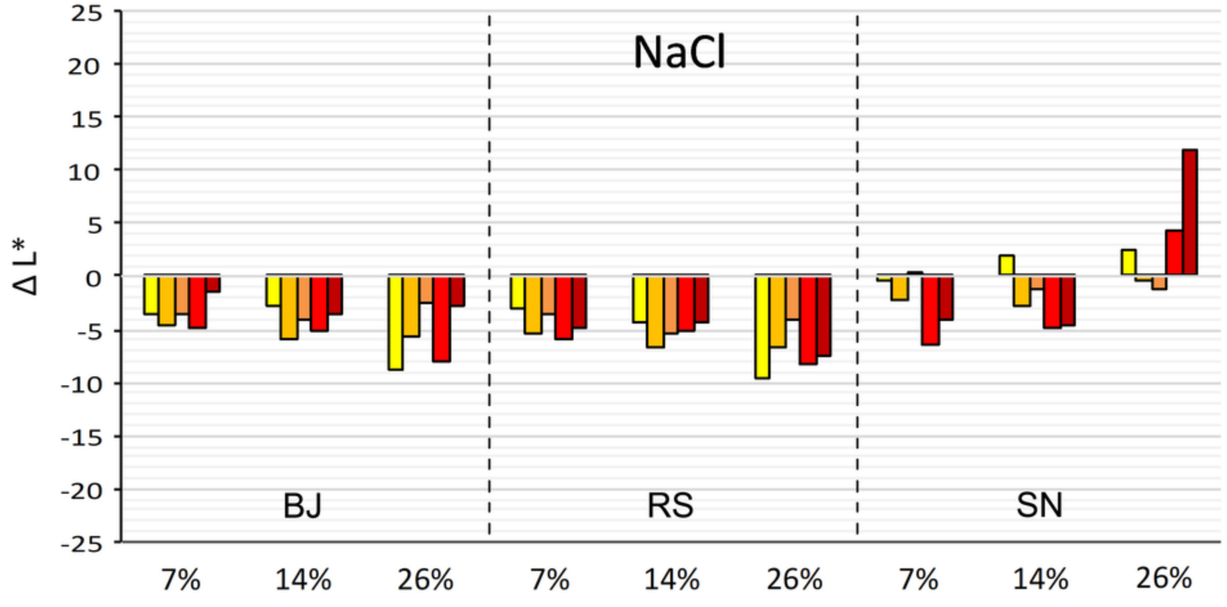

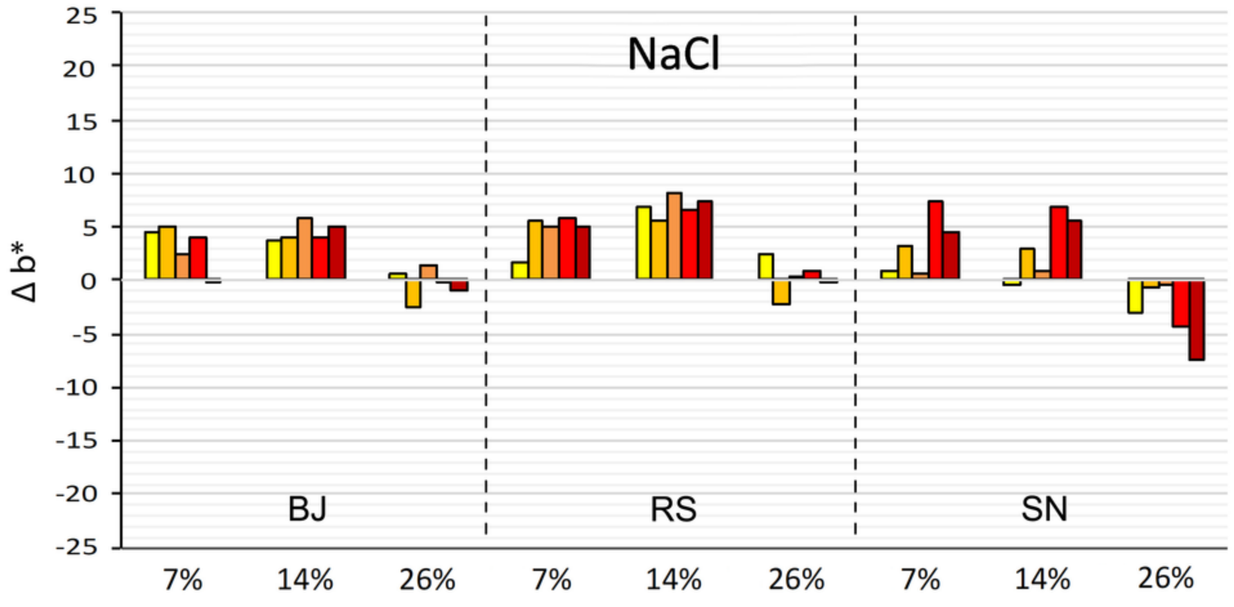

CYCLE 1 CYCLE 5 CYCLE 10 CYCLE 15 CYCLE 20

Na_2SO_4

BJ RS SN

$MgSO_4$

BJ RS SN

NaCl

BJ RS SN

ΔE*

0 5 10 15 20 25 30

7% 14% 26% 7% 14% 26% 7% 14% 26%

CYCLE 1 CYCLE 5 CYCLE 10 CYCLE 15 CYCLE 20

BJ

RS

SN

Na_2SO_4

$MgSO_4$

NaCl

Dry weight increase

20%
15%
10%
5%
0%
-5%

1 5 10 15 20

Cycle

7%

14%

26%

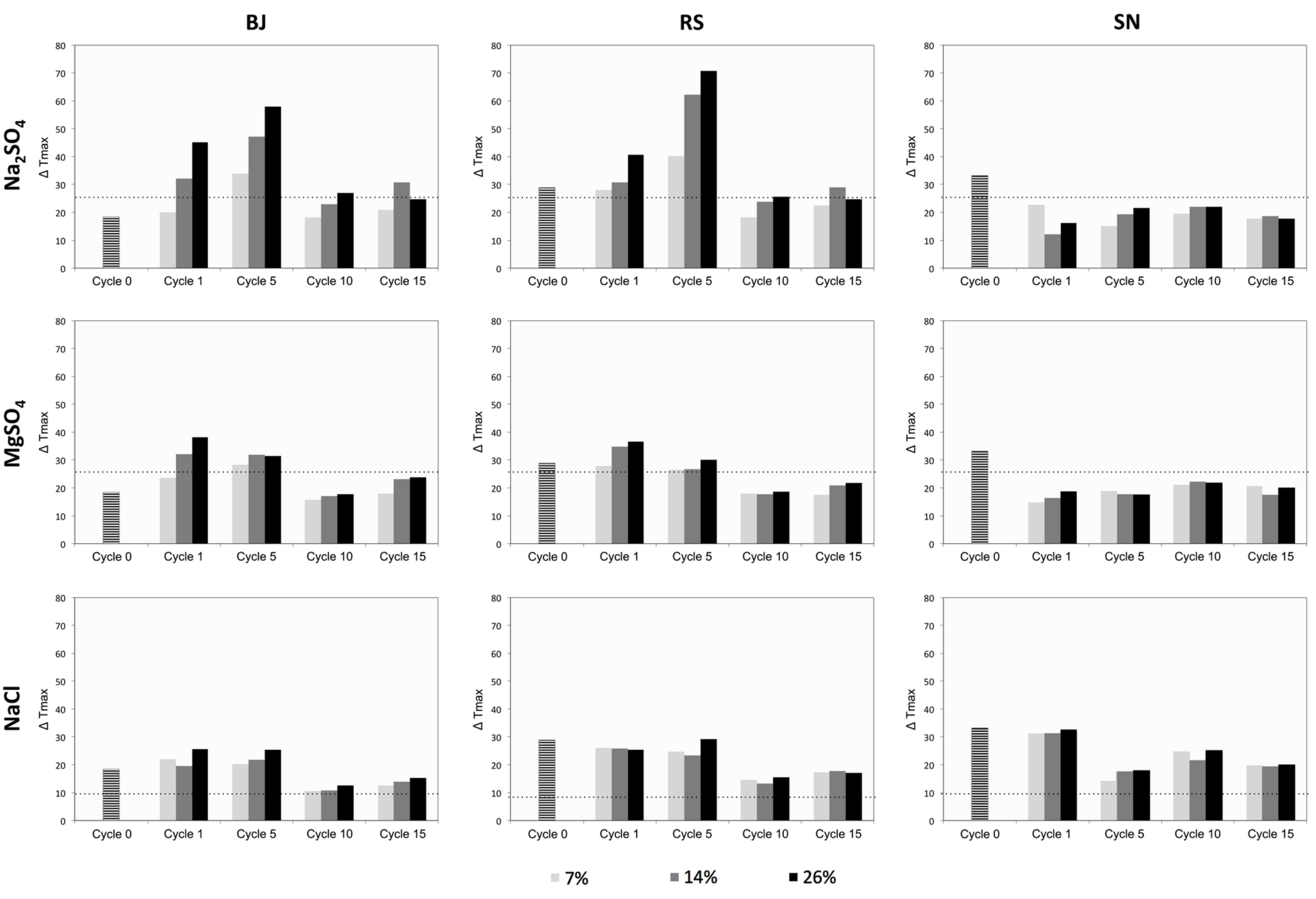
BJ
RS
SN
Na_2SO_4
$MgSO_4$
NaCl
Δ Tmax
0
10
20
30
40
50
60
70
80
Cycle 0
Cycle 1
Cycle 5
Cycle 10
Cycle 15
7%
14%
26%

BJ

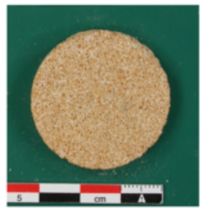

RS

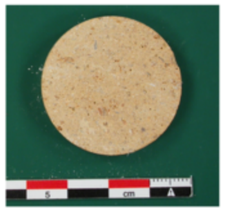

SN

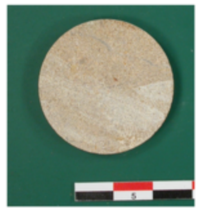

7% 14% 26% 7% 14% 26% 7% 14% 26%

Na_2SO_4

Cycle 1

Cycle 15

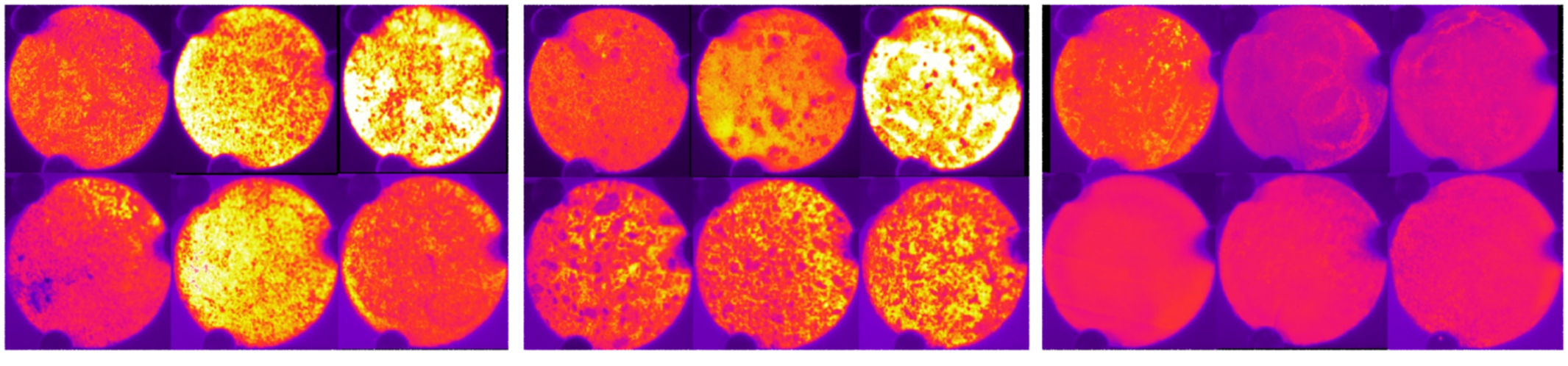

$MgSO_4$

Cycle 1

Cycle 15

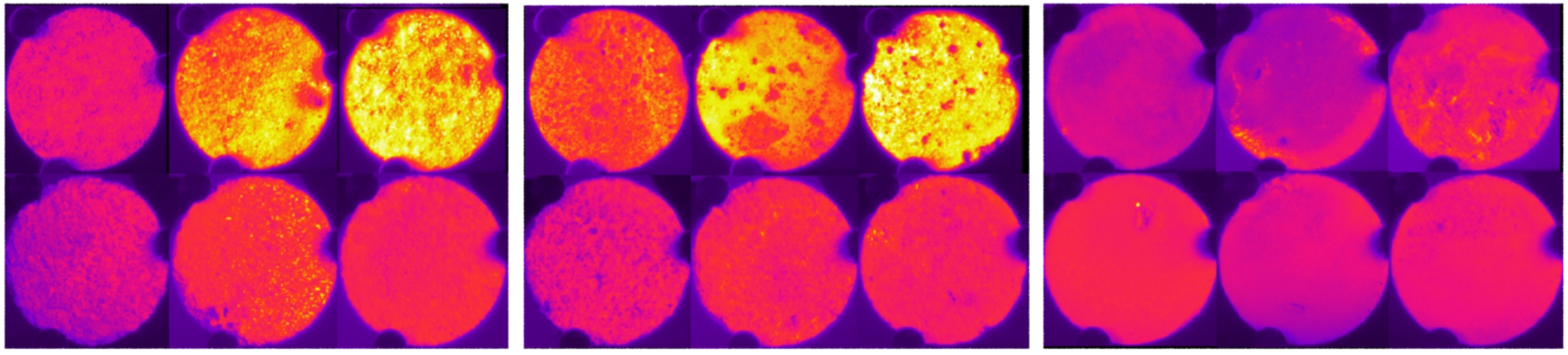

NaCl

Cycle 1

Cycle 15